Investigation of compression of indirect-drive targets under conditions of the NIF facility using one-dimensional modelling

V.B. Rozanov, G.A. Vergunova

Abstract. **The indirect compression dynamics of targets containing capsules with ablators of a plastic, high-density carbon and beryllium is simulated in the framework of a one-dimensional model based on the 1D RADIAN code. Experiments with such targets are performed on the NIF facility in the Livermore Laboratory (USA) in 2014–2018. The 1D simulation data are consistent with the results of experiments and calculations made at this Laboratory. The effect of the hard part of hohlraum radiation on capsule compression parameters is confirmed. We demonstrate the feasibility of eliminating this influence not only by selecting the hohlraum material but also by introducing admixtures into the capsule that absorb this radiation. It is shown how varying the amount of admixture in the capsule ablator varies the spectrum of the radiation that heats the DT fuel.**

Keywords: *indirect irradiation, spherical compression, laser plasma, numerical simulation.*

1. Introduction

Experiments on indirect compression of capsules confined in a cylindrical target are carried out on the megajoule National Ignition Facility (NIF), Lawrence Livermore National Laboratory, USA [1–4]. The goal is to achieve a positive thermonuclear energy yield. To date, the highest neutron yield is equal to 2×10^{16}. A comparative analysis of the experiments on targets with ablators of plastic, high-density carbon (HDC) and beryllium was performed in Refs [5–7].

The comparison of the three ablators was based on the NIF experiments on five targets [5–7]: No. 140520, a plastic target irradiated by a high foot laser pulse (CH HF); No. 151020, a plastic target in which the hohlraum was filled with low-density helium, 0.6 mg cm^{-3} instead of 1.6 mg cm^{-3} (low gas fill plastic, CH LGF); No. 161023, a target of high-density carbon in a close-to-diamond state, HDC; No. 170109, a HDC target with a big foot laser pulse (BF, the laser pulse is shortened to improve the symmetry of capsule irradiation by the X-ray radiation generated by hohlraum walls); and No. 170227, Be target. Each ablator contains layers with additions (up to 2%) of high-Z materials for controlling the heating by hard X-ray hohlraum radiation and diagnosing the mixing of Si in CH, of tungsten in HDC, and of copper in Be. The data

V.B. Rozanov, G.A. Vergunova Lebedev Physical Institute, Russian Academy of Sciences, Leninsky prosp. 53, 119991 Moscow, Russia; e-mail: vergunovaga@lebedev.ru

of numerical simulations obtained in LLNL and some experimental data are collected in Table 1.

The indirect-drive target is schematised in Fig. 1. The plastic capsule radius is equal to ~1100 μm, and the radii of HDC and Be targets are equal to ~900 μm. Among the characteristics of capsule irradiation symmetry is the hohlraum case-to-capsule ratio (CCR). Increasing the CCR the improves the absorption of laser radiation focused onto the inner domain of the target (at angles of 23.5° and 30°), but too high a CCR does not make it possible to provide a sufficiently high X-ray flux at the target. Beginning in 2014 (High foot campaign; plastic target No. 140520), the CCR increases: specifically, for plastic targets the CCR amounts to 2.55–3, for HDC to about 3, for Be to 3.7, also the hohlraum increases in height from 9.43 to 11.25 mm. The hohlraum was filled with He, whose density was equal to 1.6 mg cm^{-3} in the plastic target No. 140520, to 0.6 mg cm^{-3} in the plastic target No. 151020, and to 0.3 mg cm^{-3} in the remaining targets. This was done to weaken the scattering of laser rays and the laser-plasma interaction. The duration of laser pulses is related to the capsule dimensions and ablator thickness: it was equal to 15–13 ns for the plastic, to 6 ns for the HDC, and to 10 ns for Be. For the capsules under consideration, the laser pulse consists of three peaks, which generate three shock waves in the capsule. The last, third peak is of approximately the same duration, about 3 ns, for all three ablators. The ablator thicknesses Δ are different: $\Delta_{CH} \approx 178$ μm ($\rho_{CH} = 1.1$ g cm^{-3}), $\Delta_{HDC} \approx 65$ μm ($\rho_{HDC} = 3.5$ g cm^{-3}), and $\Delta_{Be} = 111$ μm ($\rho_{Be} = 1.85$ g cm^{-3}). The DT-fuel layer thickness was equal to 69 μm for the plastic ablators, to 53 and 41 μm for the HDC, and to 48 μm for Be.

At the LLNL the target compression was simulated in two versions. In the first one, integrated simulations model the entire indirect-drive processes: the propagation of laser beams through hohlraum, the laser-to-X-ray radiation conversion at the hohlraum walls, the capsule heating by the X-rays, the capsule implosion, and the thermonuclear fuel burn. Simulated in the second version is only the capsule compression, whose characteristics are borrowed from the more complete integrated model. Post shot modelling was performed using 2D [5–7] and 3D programmes [8]. These works considered the relative effects of different perturbation sources on capsule compression: the nonuniformity of irradiation related to the injection of laser beams into the hohlraum and its conversion to X-rays; the dimensions of the DT fill tube; the capsule support tent; and the roughness of ablator surfaces and the DT–ablator interface. To match experimental data to numerical simulations, different factors are introduced for different parts of the laser pulse. On comparing the three ablators and revealing their strong and weak points, the simu-

Table 1. Experiment parameters employed in the simulations in the present work.

Parameters	No. 140520 [5−7, 11−13]	No. 151020 [5−7, 14]	No. 161023 [5−7, 15]	No. 170109 [5−7, 16]	No. 170227 [5−7, 17]
Laser pulse energy/MJ	1.8	1.5	1.1	1.1	1.01
Laser pulse duration/ns	15	13	6	6	10
Hohlraum diameter and height/mm	5.75×9.43	6.72×11.25	5.75×10.15	5.4×10.15	6.72×11.25
He density/mg cm^{-3}	1.6	0.6	0.3	0.3	0.3
Capsule radius/μm	1125	1106	909	909	903
Inner capsule radius/μm	948	933	845	844	788
Ablator thickness/μm	178	173.1	64	65.2	111.5
Ablator density/g cm^{-3}	1.1	1.1	3.5	3.5	1.84
DT-ice layer thickness/μm	69.3	69.7	53.1	41	47.6
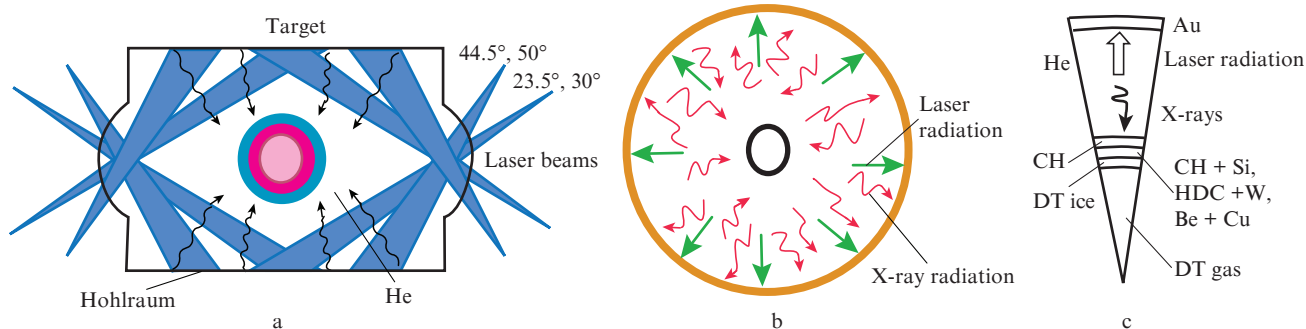
Figure 1. Schematic (a) of a cylindrical target [2] employed on the NIF and (b) of the model spherical target as well as (c) the central capsule structure.

lation data for these targets were extrapolated to full power, 500 TW and full energy, 1.8 MJ of the NIF for obtaining a high neutron yield of $10^{17}-10^{18}$.

Owing to the uniqueness of so powerful a facility as NIF, to analysis of the experiments performed on it using the codes developed in other laboratories is extremely important and topical, since the inferences drawn will broaden the understanding of the physical processes occurring in these experiments. The present work reproduces the results of these experiments and simulations in a one-dimensional formulation that has proved to be efficient [9, 10]. It turned out that the 1D model, despite its relative simplicity in comparison with the 2D model of the LLNL, reproduces the variation trends of the simulation results under target parameter variation. Numerical simulations were made of the compression of the five indicated targets as well as of the target compression for the total NIF laser energy in the framework of a one-dimensional model using the RADIAN 1D code [9, 10]. The DT fuel heating by the hard X-ray fraction of the hohlraum radiation was considered. The one-dimensional model reproduces the main results of experiments and simulation carried out at the LLNL.

2. Simulation of experiments in 1D geometry

The objective of our work is to investigate and reproduce, in the framework of the one-dimensional model of Refs [9, 10], the results of experiments and simulations performed in Refs [5−7]. The physical ground for the feasibility of one-dimensional description is the presumption that the last stage of target compression is close to the one-dimensional one. In the framework of the one-dimensional geometry there is no

way to accurately describe the injection of laser radiation into the hohlraum, the nonuniformity of capsule irradiation by the X-ray radiation generated at the hohlraum walls, the energy loss through two laser entrance holes (LEHs) (see Fig. 1a), the effect of mixing and small-scale perturbation development on the capsule compression, and the two-dimensional effects related to the capsule support tent and DT fill tube on the instability development. 1D numerical simulations nevertheless enable us to determine the main parameters of target compression and to distinguish one case from another when varying the target parameters and those of a laser pulse. It is pertinent to note that there is hardly a way to understand without numerical simulations the processes occurring in so complex a system as the indirect-drive target.

The one-dimensional simulation of indirect-drive targets is performed using the RADIAN code. In this code, two-temperature hydrodynamic equations (the equations of motion, continuity equations, the energy equations for the electron and ion components, and the equations of state for ions and electrons) are solved in combination with the multigroup spectral radiation transfer equations. The spectral radiation absorption coefficients were calculated by the THERMOS code [18] (Keldysh Institute of Applied Mathematics, RAS). Account is taken of electron−ion exchange and of the classical or suppressed Spitzer thermal conduction. The energy of laser radiation is absorbed by inverse bremsstrahlung mechanism. The laser radiation that reaches the critical density region is assumed to be completely absorbed in it. The contribution of α particles to the energy balance equation is taken into account.

In indirect-drive experiments, whose results have been published, the laser radiation is injected through the end faces

of a hohlraum cylinder and is converted to X-rays at the inner cylinder walls to fill the entire hohlraum volume and act on a capsule placed at its centre (Fig. 1). In the one-dimensional simulation the radius of a spherical hohlraum is determined by comparing the geometrical sizes of the sphere and the cylinder. The radii R_{sph} of spherical hohlraums for the indicated targets, which are used in the 1D simulations by the RADIAN code, are collected in Table 2. These radii were obtained by comparing the geometrical dimensions of a sphere and a cylinder assuming the equality of hohlraum volumes, $V_{sph} = V_{cyl}$, and the equality of hohlraum surface areas, $S_{sph} = S_{cyl}$.

A sphere and a cylinder of equal volume and equal surface area do not exist. For instance, for a 0.943-cm high cylindrical target 0.575 cm in diameter with LEHs of diameter 0.31 cm (target No. 140520), the volume and the surface area of the cylindrical hohlraum are equal to 0.245 cm^3 and 2.07 cm^2, respectively. When a sphere of the same volume is taken, the target radius is equal to 0.388 cm and the surface area of the sphere is equal to 2.22 cm^2, which exceeds the surface area of the cylindrical hohlraum by 15%. When the hohlraum and the sphere are equal in surface area, the radius of the spherical hohlraum is equal to 0.406 cm and the sphere volume to 0.281 cm^3, which exceeds the volume of the cylindrical hohlraum by 15%. For the same energy input into the hohlraum, the radiation temperature in the sphere of equal surface area will be lower by 3% than in the sphere of equal volume, which is insignificant in 1D simulations.

The laser energy injected into the spherical hohlraum cavity in one-dimensional spherical simulations is determined by comparing the energy balance equations in cylindrical and spherical geometries in dedicated 1D simulations [9]. Iterations were made to improve the fit of 1D-model simulation data to experimental ones. Varied in these iterations was the laser energy incident on the inner wall of the spherical hohlraum in order to reach a better match between the radiation temperature T_{rad} in the hohlraum cavity (Fig. 2) and the experimental data or the simulation data obtained at the LLNL and published in the literature [7].

By the point in time t, the energy balance equation for the spherical model problem is as follows [9]:

$$E_{sph}(t) = E_{rad}(t) + \int_0^t W_{cap} S_{cap} dt + E_{Au}(t),$$

where $E_{sph}(t)$ is the laser energy absorbed at the inner hohlraum wall; $E_{rad}(t)$ is the X-ray radiation energy contained in the hohlraum volume; W_{cap} is the X-ray flux on the capsule; S_{cap} is the capsule surface area; and $E_{Au}(t)$ is the energy absorbed at the inner hohlraum surface.

The laser radiation heats the inner hohlraum wall, with 64% of the laser energy being converted to X-ray radiation.
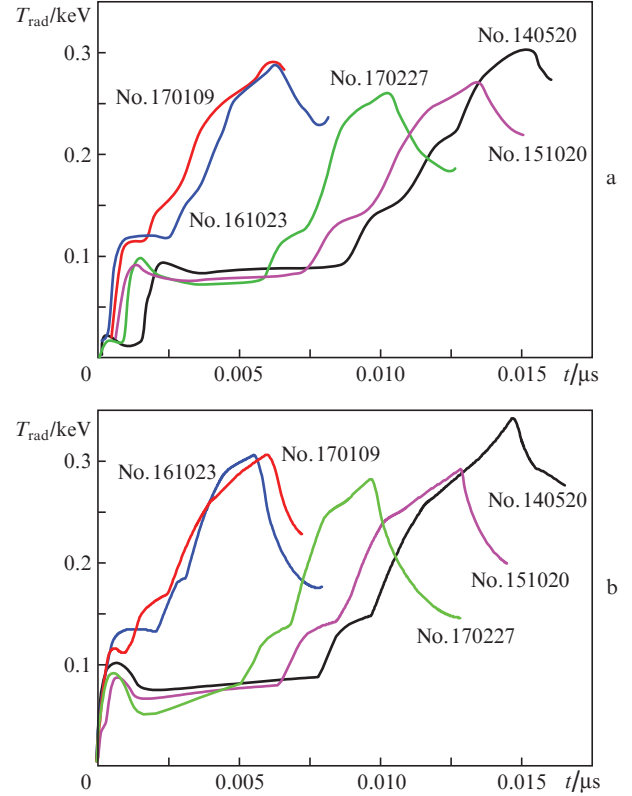
Figure 2. Comparison of the radiation temperatures in the hohlraum cavity (a) calculated for the five targets of Ref. [7] and (b) in the present work.

Part of this X-ray radiation is incident on the capsule and heats it. Part of X-rays passes by the capsule to additionally heat the inner hohlraum surface. Therefore, the inner hohlraum surface is heated not only directly by the laser radiation but also by the generated X-ray radiation. The laser energy absorbed in the inner hohlraum wall (Au) and in the central capsule (CH, HDC, or Be), is determined directly in the simulation for a given time dependence of laser pulse intensity. For instance, in the simulation of shot No. 140520, as a result of X-ray production, transfer and absorption in the hohlraum an X-ray energy of 0.15 MJ finds its way into the capsule by the instant of laser pulse termination ($t = 15$ ns), which is consistent with the data obtained at the LLNL [2].

Table 3 presents the data of some simulations for five targets in the one-dimensional geometry under consideration and their comparison with the data of experiments and simulations carried out at the LLNL. The 1D simulation data presented here correspond to the range of the data of experi-

Table 2. Geometrical dimensions of cylindrical and spherical hohlraums.

Parameters	No. 140520	No. 151020	No. 161023	No. 170109	No. 170227
Hohlraum diameter/cm	0.575	0.672	0.575	0.54	0.672
Hohlraum height/cm	0.943	1.124	1.01	1.015	1.124
LEH diameter/cm	0.31	0.391	0.337	0.34	0.391
R_{sph}/cm ($V_{sph} = V_{cyl}$)	0.3881	0.4566	0.3971	0.3814	0.4566
R_{sph}/cm ($S_{sph} = S_{cyl}$)	0.4060	0.4756	0.4151	0.3988	0.4756

Table 3. Results of experiments with targets containing plastic, HDC and Be capsules, as well as data of numerical simulations carried out at the LLNL and those made by the 1D RADIAN mode.

Parameters	No. 140520	RADIAN (hf028)	No. 151020	RADIAN	No. 161023	RADIAN	No. 170109	RADIAN	No. 170227	RADIAN
Peak radiation temperature/eV	305–322	329	273	280	288	298	292	300	264	280
Compression time/ns	15.91	15.3	–	14.73	–	7.55	–	7.38	–	12.52
Plasma confinement time/ps	145	152	–	286	–	185	135	186	–	177
Neutron yield/10^{15}	9	7.6	3.5	3.8	4.7	3.8	2.3 Sim 4.07 (LLNL)	3.7	0.4 Sim 0.8 (LLNL)	0.7
Peak compression velocity/km s^{-1}	367–387	365	345	378	375–382	386	389–411	390	332–345	281
$\rho\Delta R$/g cm^{-2}	0.14	0.16	–	0.16	–	0.11	0.15	0.11	–	0.09
Ion temperature/keV	5.54	5.1	4	4.3	4.5	4.5	4.2	3.8	3.4 Sim 4.5 (LLNL)	3
Adiabatic exponent	2.3	2.9	2.1	4.6	2.6	3.6	3.9	2.7	2.2	3.1
Non-evaporated ablator part (%)	5.2	11	8.2	10	5	12	6.6	9	5.9	22

Note: ρ is the density and ΔR is the thickness of compressed domain.

ments and simulations performed at the LLNL. Specifically, the difference in the peak radiation temperature in the hohlraum cavity in the 1D simulation does not exceed 6% for all simulations. In the literature we found the collapse time, 15.91 ns, only for experiment No. 140520, which is equal to 15.3 ns in our simulations. The plasma confinement time in the 1D simulation of case No. 170109 differs by 40% from the data obtained at the LLNL. The peak fuel compression velocities differ from those calculated at the LLNL by less than 10% for the plastic, by less than 5% for HDC, and by less than 19% for the Be capsule. The $\rho\Delta R$ product differs by 14% for the plastic and by 27% for the HDC. The ion temperatures are consistent with the data obtained at the LLNL. A relatively strong difference is observed for the non-evaporated ablator mass, especially for Be. It is nevertheless safe to say that the one-dimensional model in use adequately reproduces the main parameters of compression for plastic, HDC and Be capsules in the experiments with indirect-drive targets.

To achieve a high DT fuel density for a minimal input energy, the capsule compression by an X-ray pulse should proceed isentropically. The main sources of fuel heating are shock waves. Electron thermal conduction, the fast electrons generated in the instability region, and the preheating by hard X-rays increase the entropy of the DT fuel under compression [2]. We cannot include two-dimensional effects, which are determinative for so complex a structure as an indirect-drive target.

In the 1D simulations by the RADIAN model, the hohlraum radiation delivers additional energy to the DT fuel. The adiabatic (isentropic) exponent is calculated as the ratio between the pressure at a given density and the pressure of degenerate Fermi gas ($\alpha = p/p_{\mathrm{F}}$) at the moment of highest kinetic energy [19]. In the simulations by the 1D RADIAN code the adiabatic exponent is greater than in the simulation carried out at the LLNL (with the exception of the simulation for target No. 170109). This is due to a greater entropy increase, which arises from the energy input into the fuel caused by hohlraum radiation.

We consider the effect of the energy contribution made by hohlraum radiation on the parameters of capsule compression by the example of No. 140520 experiment simulation. The general picture of target compression is represented by the $R-t$ diagram plotted in Fig. 3. Used for the specified experiment is a hohlraum filled with He of density 1.6 mg cm^{-3}, which contains a capsule with an external diameter of 2.25 mm and an ablator thickness of 178 μm. DT ice of thickness 69.3 μm is frozen inside of the capsule (see Table 1). At the CH–DT-ice interface the ablator contains a 54-μm thick Si-doped layer for mixing diagnostics and for controlling the absorption of hohlraum radiation.

The 9.43-mm long cylindrical hohlraum 5.75 mm in diameter is replaced with a spherical hohlraum of radius 3.88 mm. The duration of the last, third peak of laser radiation is equal to 3 ns (Fig. 3a). By the point in time $t = 14$ ns the DT–ablator boundary passes 2/3 of the path to target compression. The density, electron temperature and radiant flux profiles are plotted in Fig. 3b for this point in time. Incident on the capsule at this point in time is the X-ray flux W_{cap}, which amounts to 54% of the laser radiation flux.

Figure 4 shows the spectral radiation fluxes in the range 0–6 keV at the CH–DT boundary for No. 140520 experiment simulations. Varied in these simulations was the ablator absorption coefficient to investigate the effect of hohlraum radiation on the parameters of capsule compression (Table 4). In the simulation hf032 the Si layer was removed, which resulted in a ~22% increase in the energy of the hohlraum radiation with $hv > 2$ keV that reached DT in comparison with that in the nominal simulation hf028. The adiabatic exponent, which is determined at the point in time when the kinetic energy is at its maximum, increased from 2.9 to 5.6.

In the simulation hf033 the ablator absorption coefficient was increased by 20% relative to the absorption coefficient in the simulation hf028. In this simulation the hohlraum radiation energy supplied to the DT fuel is 28% lower, the neutron yield is higher, and the adiabatic exponent lowers to 1.8.

a

b
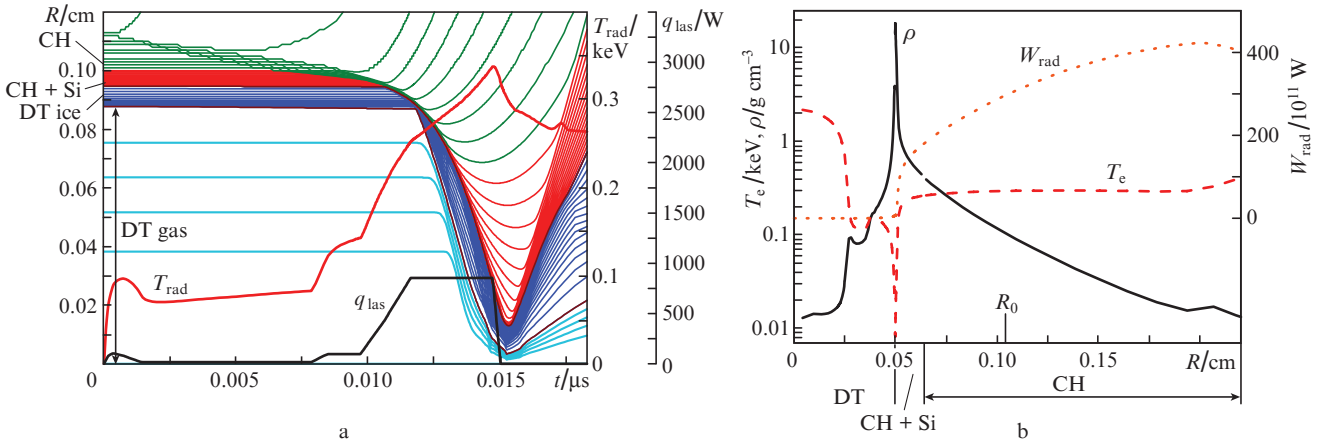
Figure 3. (Colour online) (a) $R-t$ diagram of internal capsule compression in the No. 140520 experiment simulation (q_{las} is the power of the laser pulse consisting of three peaks) as well as (b) profiles of the density ρ, electron temperature T_e and radiant flux W_{rad} at the point in time $t = 14$ ns (R_0 is the initial capsule radius).
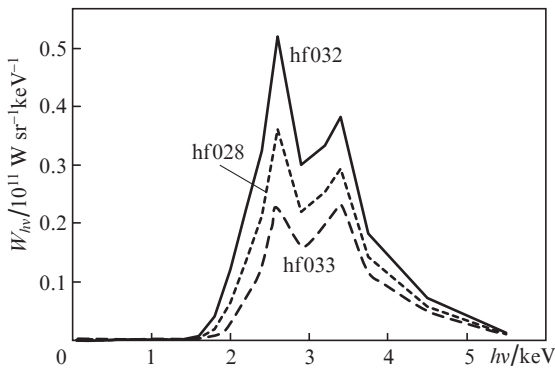
Figure 4. Spectral radiant fluxes $W_{h\nu}$ at the CH–DT boundary at the point in time $t = 14$ ns.

Table 4. Effect of ablator absorption coefficient on the target compression.

Simulation	Variation of hohlraum radiation energy supplied into DT fuel relative to the nominal energy	Neutron yield/10^{15}	Adiabatic exponent
hf028	0	7.6	2.9
hf032	+22%	5.5	5.6
hf033	−28%	12	1.8

Also, simulations were made in which the Si layer thickness in the ablator was varied. Table 5 shows the neutron yield in relation to the thickness of this layer. One can see that it depends almost linearly on the layer thickness. Therefore, inaccuracies in the knowledge of optical properties of substances can significantly change the results of numerical simulations.

The emission spectrum of the hohlraum, which consists of gold (Au), has a local peak (Fig. 5a) in the 2–3 keV range due to the lines arising from 4–3 transitions (for instance, the $M_{\alpha 1}$ line at an energy of 2.1 keV) and transitions at the bound-free edge in the same range. On placing a layer of depleted uranium (DU) in gold in our simulations, the spectral radiant flux lowers three-fold in the 2–3 keV spectral range. The radiant flux becomes lower, because the M_α lines of uranium are at higher spectral energies: for instance, the $M_{\alpha 1}$ line is radi-

Table 5. Neutron yield in relation to the Si layer thickness.

Si layer thickness/μm	Neutron yield/10^{15}
27	6.1
54	7.6
81	8.7

ated at 3.2 keV. In addition, to attain the same isoelectronic state in uranium (with nuclear charge $Z_U = 92$) requires a higher energy input than in the case of gold ($Z_{Au} = 79$). The $h\nu$

a

b
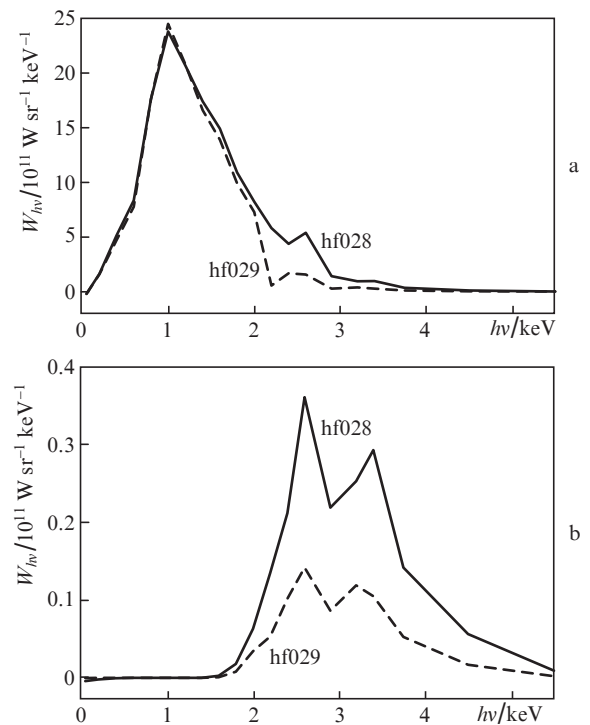
Figure 5. Emission spectra of the hohlraum of gold (solid curves) and of gold containing a layer of depleted uranium (dashed curves) (a) for the spectral radiant fluxes incident on the capsule (He–CH boundary) and (b) for those incident on the DT fuel (CH–DT boundary). The curves are plotted for the point in time $t = 14$ ns.

> 2 keV radiation accounts for ~13% of the total spectral energy of gold hohlraum radiation (for a temperature $T_{rad} \approx$ 300 eV). Despite the addition of Si to the ablator for absorbing external radiation and preventing the DT fuel preheating, the radiation of the hv > 2 keV spectral domain penetrates through the ablator and finds its way to DT in the case of gold hohlraum. Figure 5b shows the spectral fluxes of hohlraum radiation that reach the DT fuel. For a gold hohlraum the spectral flux in the hv > 2 keV domain is approximately three times greater than in the case of hohlraum with the addition of a DU layer. Adding DU to gold hohlraum has the effect that the neutron yield increases three-fold in No. 140520 experiment simulations.

This result is consistent with that of Ref. [20] and confirms the validity of employing the 1D model under discussion for simulating indirect-drive targets. Therefore, the hard part of the heating spectrum may be attenuated by selecting the hohlraum material. Another way of controlling the spectrum of radiation that heats the DT fuel is to change the ablator properties, as shown in Ref. [21] and in the present work.

3. Simulation of targets proposed for future experiments

Proceeding from theoretical investigations and numerical simulations of experimental data, targets intended for obtaining a neutron yield of $10^{17} - 10^{18}$ were proposed in Refs [5–7] for each of the ablator materials (plastic, HDC, and Be).

Experiments with these targets will be supposedly carried out with the use of the total energy (1.8 MJ) and full peak power (370–500 TW) of the NIF. It is also planned to place the three capsules in the hohlraums of the same size (cylinder height, 11.25 mm; hohlraum diameter, 6.72 mm; and diameter of the LEHs, 3.64 mm). The hohlraum will be filled with helium of density 0.6 mg cm^{-3}. The hohlraum wall structure is as follows. A 7-μm thick DU layer on the inner side of the hohlraum is coated with a 0.7-μm thick gold layer. Added on the outer side is a 22.3-μm thick gold layer, so that the total thickness (30 μm) is the same as for purely golden hohlraums. The thin layer of gold on the inner side of the hohlraum prevents the DU layer from oxidation and hinders its vaporisation prior to the arrival of the main pulse of laser radiation. All these capsules contain ~185 mg of DT ice, the CCR is equal to ~3 for the three ablator versions, and the capsule radius is equal to ~1110 μm. The duration of the laser pulse is equal to 11 ns for the plastic, to 8.3 ns for HDC, and to 16.1 ns for Be.

In the present work we performed 1D numerical simulations for these targets oriented to future experiments. The results of our simulations with those made at the LLNL [5–7] are compared in Table 6. The neutron yield calculated by the 1D model is consistent with the data of LLNL simulations for all three targets. For plastic and HDC ablators, the peak fuel velocity is lower than that obtained at the LLNL, and for the Be ablator the velocity is higher. In the 1D simulations the peak kinetic energy of the fuel is lower than in the LLNL simulations. The plasma confinement time in the CH and HDC capsules agrees nicely with the LLNL simulation data (0.66 ns and 1.38 ns, respectively), while for Be it turns out to be two times longer: 0.4 ns and 0.98 ns. In our simulations the adiabatic exponent for the plastic capsule is somewhat higher (3.2 in comparison with 2.7) and lower for HDC and Be (1.2 in comparison with 2.4 for HDC and 1.3 in comparison with 1.6 for Be). On the whole, the data of 1D model simulations agree with the data obtained in the LLNL simulations.

Figure 6 shows the plastic target density profiles at the point in time corresponding to the highest kinetic energy (in the simulations by the RADIAN code this is the point in time t = 11.16 ns). The target densities are in the same range, but their spatial distributions are different. This is supposedly because the equations of state of the ablator and the DT fuel we used were different from those employed in LLNL codes. Agreement with the data of the one-dimensional LLNL simulations was reached when the ablator absorption coefficient was increased by a factor of two. Therefore, our 1D model provides a correct description of the compression and implosion of target capsules under indirect compression, as well as the trends in these processes when varying the parameters of the capsules and hohlraum.

4. Conclusions

The results of experiments in the indirect compression of capsules with plastic, HDC and Be ablators were investigated and reproduced with the use of a well-established one-dimensional model [9, 10]. The 1D RADIAN code simulations are

Table 6. Simulation data for optimised plastic, HDC and Be targets for LLNL and RADIAN mathematical codes.

Parameters	Plastic		HDC		Be	
Laser pulse duration/ns	11		8.3		16.1	
Capsule radius/μm	1125		1100		1120	
Ablator thickness/μm	175		84		142	
DT ice layer thickness/μm	69		59		64	
	LLNL	RADAN	LLNL	RADAN	LLNL	RADAN
Neutron yield						
1D simulation	$(1-1.4) \times 10^{17}$	1.4×10^{17}	$(5-7) \times 10^{17}$	2.5×10^{17}	$(3.7-3.8) \times 10^{18}$	2.7×10^{18}
2D simulation	$(1.3-8) \times 10^{16}$	–	$(2.8-5) \times 10^{17}$	–	$2 \times 10^{16}-1.6 \times 10^{18}$	–
Peak velocity/km s^{-1}	374	343	402–412	368	350	363
Maximal kinetic fuel energy/kJ	13	9.8	14.5–15.3	11	11.1	9.5
Confinement time/ns	0.65–0.8	0.66	1.48–1.55	1.38	0.4	0.98
Ion temperature/keV	3.4–3.75	3.3	4.6	4	3.8–4	3.7
Adiabatic exponent	2.73	3.2	2.45–2.52	1.2	1.6	1.3
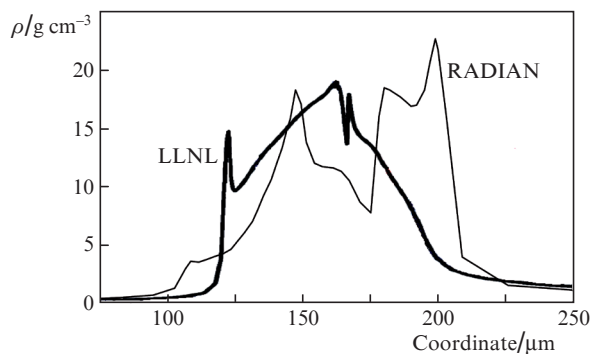
Figure 6. CH target density profiles at the point in time corresponding to the highest kinetic energy, which were obtained in our work and at the LLNL.

in reasonable agreement with the data of experiments and simulations carried out at the LLNL. The one-dimensional model correctly describes the target capsule compression as well as the trends in this process when varying the parameters of the target and the laser pulse.

The data of target capsule compression simulations for these ablators, extrapolated to the total energy of the NIF, also correspond to the data of simulations performed at the LLNL [5–7]. This gives us confidence that the one-dimensional model we use adequately conveys the trends of indirect compression of targets and its application makes sense. The existing uncertainties in the properties of ablator and DT fuel materials have effect on the equations of state in use and on optical constants. As a result, uncertainties in the properties of these materials affect the results described.

The effect of hard X-ray hohlraum radiation on the growth of adiabatic exponent in the capsule compression has been confirmed in the framework of the 1D model. We have demonstrated the method for controlling the spectrum of capsule-compressing radiation, which consists in changing the properties of the ablator. Earlier in Ref. [21] it was shown that layers of heavy elements (Cu) can be used in the capsule to absorb the hard part of the X-ray radiation of the hohlraum and achieve ignition of the DT fuel.

References

1. Lindl J. *Phys. Plasmas*, **2**, 3933 (1995).
2. Lindl J.D., Amendt P., Berger R.L., et al. *Phys. Plasmas*, **11**, 339 (2004).
3. Moses E.I. *J. Phys.: Conf. Ser.*, **112**, 012003 (2008).
4. Moses E.I., Boud R.N., Remington B.A., Keane C.J., Al-Ayat R. *Phys. Plasmas*, **16**, 41006 (2009).
5. Clark D.S., Kritcher A.L., Yi S.A., Zylstra A.B., Haan S.W., Weber C.R. *Phys. Plasmas*, **25**, 032703 (2018).
6. Kritcher A.L., Clark D., Haan S., Yi S.A., Zylstra A.B., Callahan D.A. *Phys. Plasmas*, **25**, 056309 (2018).
7. Haan S.W., Kritcher A.L., Clark D.S., Yi S.A., Zylstra A.B., Ralph J.E., Weber C.R. *Report LLNL-TR-741418* (2017).
8. Clark D.S., Weber C.R., Milovich J.L., et al. *Phys. Plasmas*, **26**, 050601 (2019).
9. Rozanov V.B., Vergunova G.A. *JETP*, **121**, 747 (2015) [*Zh. Eksp. Teor. Fiz.*, **148**, 857 (2015)].
10. Rozanov V.B., Vergunova G.A. *JETP*, **124**, 182 (2017) [*Zh. Eksp. Teor. Fiz.*, **151**, 210 (2017)].
11. Döppner T., Callahan D.A., Hurricane O.A., et al. *Phys. Rev. Lett.*, **115**, 055001 (2015).
12. Hurricane O.A., Callahan D.A., Casey D.T., et al. *Nature Phys.* (2016), DOI: 10.1038/NPHYS3720.
13. Baker K.L., Thomas C.A., Casey D.T., et al. *Phys. Rev. Lett.*, **121**, 135001 (2018).
14. Hinkel D.E., Berzak Hopkins L.F., Ma T., et al. *Phys. Rev. Lett.*, **117**, 225002 (2016).
15. Divol L., Pak A., Berzak Hopkins L.F., et al. *Phys. Plasmas*, **24**, 056309 (2017).
16. Casey D.T., Thomas C.A., Baker K.L., et al. *Phys. Plasmas*, **25**, 056308 (2018).
17. Zylstra A.B., Yi S.A., MacLaren S., et al. *Phys. Plasmas*, **26**, 052707 (2019).
18. Nikiforov A.F., Novikov V.G., Uvarov V.B. *Kvantovo-statisticheskie modeli vysokotemperaturnoi plazmy* (Quantum Statistical Models of High-Temperature Plasma) (Moscow: Fizmatlit, 2000).
19. Herrmann M.C., Tabak M., Lindl J.D. *Nucl. Fusion*, **41** (1), 99 (2001).
20. Dewald E.L., Tommasini R., Meezan N.B., et al. *Phys. Plasmas*, **25**, 092702 (2018).
21. Rozanov V.B., Vergunova G.A. *JETP*, **127**, 786 (2018) [*Zh. Eksp. Teor. Fiz.*, **154**, 919 (2018)].